JOURNAL OF PROPULSION AND POWER
Vol. 19, No. 4, July–August 2003

Low-Engine-Order Excitation Mechanisms in Axial-Flow Turbomachinery

C. Bréard*
Analytical Methods, Inc., Redmond, Washington 98052
J. S. Green†
Rolls–Royce, plc., Derby, England DE24 8BJ, United Kingdom
and
M. Imregun‡
Imperial College London, London, England SW7 2BX, United Kingdom

One particular regime of forced response, occurring at much lower frequencies than the blade-passing frequency, is the so-called low-engine-order (LEO) forced response. The source of LEO excitation is a loss of symmetry in the flow, such as that caused by stator blade throat width variations, flow exit angle variations, perturbations in the passage cooling flow, or temperature distortions. Using a 3D integrated time-domain aeroelasticity code, parametric forced response studies were conducted for a high-pressure turbine stage with 36 stator and 90 rotor blades. Both whole-annulus and sector models were used to investigate the effects of individual and combined LEO parameters. For individual parameters, the amplitude of the excitation was, proportional to the imposed variation. For combined cases, the total excitation was found to be determined by the phasing between the individual excitations. A ballpark comparison suggested that LEO and blade-passing forced response vibration amplitudes were similar for typical variations of the controlling LEO parameters.

Introduction

A PRIMARY mechanism of turbomachinery blade failure is high-cycle fatigue caused by vibrations at levels exceeding the material endurance limits. Such a situation occurs when a forcing function, created by various distortions in the high-speed airflow, acts on a blade row with a frequency and spatial distribution similar to a natural mode of vibration of the assembly. What is of interest is the strength of the blade response under the effect of the unsteady aerodynamic forcing, hence, the term forced response. (Blade mistuning, or small blade-to-blade differences due to manufacturing tolerances, can have significant influence on forced response levels.[1,2] Here, it is proposed to deal with tuned rotor assemblies only.) During the design and development of gas turbines, it is essential to identify components that are likely to suffer high vibration with a view to minimize their response amplitude to prevent high-cycle fatigue failures.

From the outset, it is appropriate to distinguish between two types of forced response. The first type, blade-passing forced response, is due to the excitation forces generated by the rotation of the bladed system past a pressure field, the strength of which varies periodically with angular position around the turbine. Such flow variations are mainly caused by the stator blades, which act as upstream obstructions, and the rotor blades experience their wakes as time-varying forces with a frequency (or periodicity) based on the rotation speed. The spatial distribution of the forcing function will primarily be determined by the number of upstream stator blades and by its aliases with respect to the rotor blades. A Fourier transform of this forcing function will reveal harmonics that will typically excite high nodal diameter modes because their actual order is related to the blade numbers in the rotor/stator row of interest. Turbomachinery designers rely on Campbell diagrams (or their variants) that indicate the likelihood of encountering forced response resonances of the first type within the operating range. In principle, it is then possible to design the rotor wheels away from the primary resonances, subject to being able to predict the assembly's dynamic behavior to a required degree of accuracy. However, an accurate prediction of absolute vibration levels for rotor blades is fraught with many difficulties because of uncertainties in structural damping, blade mistuning effects, and multi-blade-row interactions.

The second type of forced response, the main subject of this paper, is somewhat more difficult to deal with because the controlling parameters and the exact excitation mechanism are poorly understood. However, the unsteady aerodynamic forcing function is known to be composed of low-order harmonics because it is responsible for exciting low-order nodal diameter assembly modes, hence, the term low-engine-order (LEO) forced response. The main characteristics of the LEO forced response in turbine assemblies can be summarized as follows.

1) It occurs at high speed and temperature, and it tends to persist throughout the engine, affecting high-pressure (HP), intermediate-pressure (IP), and low-pressure (LP) turbines.

2) It excites low nodal diameter fundamental blade modes that exhibit higher vibration levels, thus increasing the likelihood of blade failures.

3) A large degree of variability is observed from engine to engine. The same is also true of the particular LEO harmonic that produces the highest response in a given nominal engine.

4) Industrial experience suggests that any loss of symmetry might give rise to LEO forced response. The following parameters are thought to be the most significant ones: inherent nonuniform spacing of the stator blades (or throat width variation), flow exit angle variations, axial gap changes between the rotor and stator blades, general unsteadiness through the engine, density variation due to combustion effects, blade numbers through several stages, and effects due to burner variability.

5) There is little correlation between some experimental observations, although it is recognized that significant measurement errors may exist. For instance, the LEO response due to burner blockage seems to remain unchanged in some engines, whereas it may be significantly lower or higher in other engines.

Received 29 July 2002; revision received 7 April 2003; accepted for publication 7 April 2003.

*Senior Research Scientist, 2133 152nd Avenue Northeast.
†Principal Technologist, Mechanical Methods, P.O. Box 31.
‡Professor, Mechanical Engineering Department, Exhibition Road.

6) On rig and engine tests, many of the highest measured responses in the running range are observed to be due to LEO excitation. Such situations require expensive modifications in relatively late stages of the design cycle. Because the controlling mechanism is poorly understood, the use of friction dampers (small devices that dissipate energy by friction, usually placed at blade roots) to reduce the response levels is often the only route available to the designer.

7) It is possible that LEO excitation may influence or even interact with LP turbine blade flutter, the latter being another aeroelastic phenomenon associated with low nodal diameter assembly modes.

8) A different type of LEO excitation, arising from inlet distortions, occurs in compressor assemblies, especially in the case of military aircraft because engines are often fuselage mounted, requiring complex intakes for low observability. Because the exact inlet geometry and other upstream obstacles are known, the prediction of the ensuing response is relatively straightforward. Similarly, the asymmetry of civil aeroengine intake ducts may create LEO forcing and the crosswind effects may be significant.

9) Finally, mechanisms other than loss symmetry may also be responsible for LEO excitation. In both turbine and compressor assemblies, blade number differences across several bladerows will produce low-order harmonics, though the actual amplitudes will usually be small.

Previous forced response studies have almost exclusively dealt with classical forced response. Chiang and Kielb,[3] who present an industrial design prediction system, also review much of the research in this area. The usual approach is to solve non-linear Euler or Navier–Stokes equations for the blade row of interest and to simulate the disturbance (wake or potential) moving past at blade passing velocity. Hodson[4] and Giles[5] used the inviscid Euler equations to predict wake–rotor interaction. Similar work is also reported by Fransson and Pandolfi[6] and by Gerolymos.[7] A full stator/rotor interaction model using Navier–Stokes equations was developed in three dimensions by Rai.[8] A study of varying the blade numbers is reported by Korakianitis.[9,10] Results from some of the cited models are compared with experimental data in the paper by Manwearing and Wisler.[11] One of the first LEO forced response studies is described by Manwearing and Kirkeng.[12] The effects of a non-uniform temperature distribution at the LP turbine inlet were reported for an industrial gas turbine. A review of forced response methodologies is given by Sayma et al.,[13] who also described a state-of-the-art formulation. A large-scale multi-blade-row numerical model of an HP turbine was used by Vahdati et al.[14] to predict the LEO harmonics arising from stator blade throat width variations. It was found that such variations could cause significant increase in the vibration levels.

The primary aim of this work is to understand the contribution of each parameter to the strength of unsteady aerodynamic excitation that gives rise to LEO forced response. This overall aim can only be met if all parameters of interest are present in the model as one is probably looking for certain combinations of the main controlling parameters that need to be determined. Accordingly, the main purpose of this paper is to present a systematic study of the LEO forced response by considering the individual and combined effects of the controlling parameters for LEO excitation, namely, stator blade throat width variation, flow exit angle variation, temperature distortion at stator outlet, blocked burners, and cooling flow variations.

Overview of the Aeroelasticity Methodology

The details of the unsteady flow and aeroelasticity code that will be used in this study have already been described by Sayma et al.[12,13,15,16] and Barakos et al.[17] and will not be repeated here. However, for the sake of completeness, a brief overview of the aeroelasticity modeling methodology will be given.

The flow domain is described using general unstructured grids of three-dimensional elements such as tetrahedra, hexahedra, and wedges, a feature that offers great flexibility for modeling complex shapes. The actual blade geometry is described using the semistructured meshing methodology of Sbardella et al.[18] The individual elements can have any number of boundary faces, and the flow variables are stored at the vertices. The numerical scheme is second-order accurate in space for tetrahedral meshes. For prismatic and hexahedral cells, the scheme is still second-order accurate for regular cells with right angles. In the worst case of a highly skewed cell, the scheme will reduce to first-order accuracy. However, hexahedral meshes are usually generated in boundary layer, where orthogonality results in regular cells. Similarly, prismatic cells are usually generated in a structured manner by projecting triangular meshes on radial layers and then connecting them. Highly skewed meshes are unlikely to occur in these situations.

The computational domain is stored using an edge-based data structure that results in a central difference scheme for the advection terms that is stabilized using a mixture of second- and fourth-order matrix artificial dissipation. The time stepping is done in an implicit fashion, and, hence, relatively large Courant–Friedrichs–Lewy numbers, typically 10–30 in the current study, can be used without creating numerical instabilities in the solution algorithm. The so-called dual-time-stepping procedure is used for unsteady flow calculations. The time accuracy is guaranteed by the outer iteration level, where the time step is fixed throughout the solution domain, whereas the inner iterations can be performed using traditional acceleration techniques such as local time stepping and residual smoothing. In any case, the selection of the time step is dictated by the physics of the phenomena under investigation. For forced response calculations, a vibration cycle needs to be captured with enough points, for example, about 250 per period. The code can be run in viscous mode via Reynolds averaged Navier–Stokes equations with Baldwin–Barth, Spalart–Allmaras or q–zeta turbulence models. However, an inviscid flow representation was used in the current study.

The structural model is based on a linear modal model, the mode shapes and natural frequencies being obtained via standard finite element analysis techniques. The mode shapes are interpolated from the structural mesh onto the aerodynamic mesh because the two discretization levels are unlikely to be coincident. Boundary conditions from the structural and aerodynamic domains are exchanged at each time step, and the aeroelastic mesh is moved to follow the structural motion using a spring analogy algorithm.

Throughout the paper, the strength of the excitation will be monitored using the concept of modal force, which is the product of the unsteady fluid pressure with a given structural mode shape. Such a quantity, which represents the strength of the unsteady forcing in a particular mode of vibration, can best be visualized by considering a rigid-body motion where the blade is plunging only. In this case, the modal force can be considered to be the unsteady lift on the blade. For a given mode, the strength of the modal force depends on the pressure perturbation and the correlation between the perturbation shape and the structural mode shape. In this particular study, modal force time histories were found to reach periodic convergence after a few vibration cycles.

Case Studies

The case study is conducted for an HP turbine stage of a large-diameter aero-engine. The stage has 36 stator and 90 development-standard rotor blades with an aspect ratio of 0.4. The resonance of interest occurs for the first flap (1F)/six nodal diameter (ND) mode, which is susceptible to six engine-order (EO) excitation at around 98% speed. Experimental evidence indicates that significant vibration response occurs in this mode, although there is a lack of sufficiently accurate data relating parameter perturbation to the ensuing response increase with adequate resolution. Therefore, a range of representative values will be used for the parameter studies to see if the predicted LEO excitation will fall into the expected bands of measured behavior. The corresponding Campbell diagram is given in Fig. 1. Because of the matching stator/rotor blade numbers, wherever possible, the analysis was conducted for a typical sector of 6 stator and 15 rotor blades (Fig. 2).

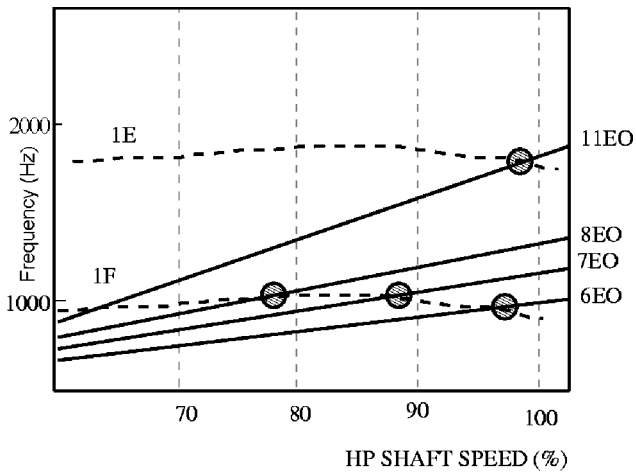

Fig. 1 Campbell diagram showing possible LEO resonances.

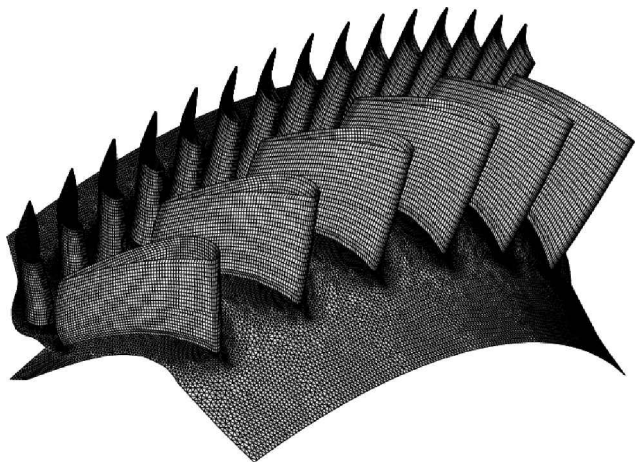

Fig. 2 Typical computational sector with 6 stator and 15 rotor blades.

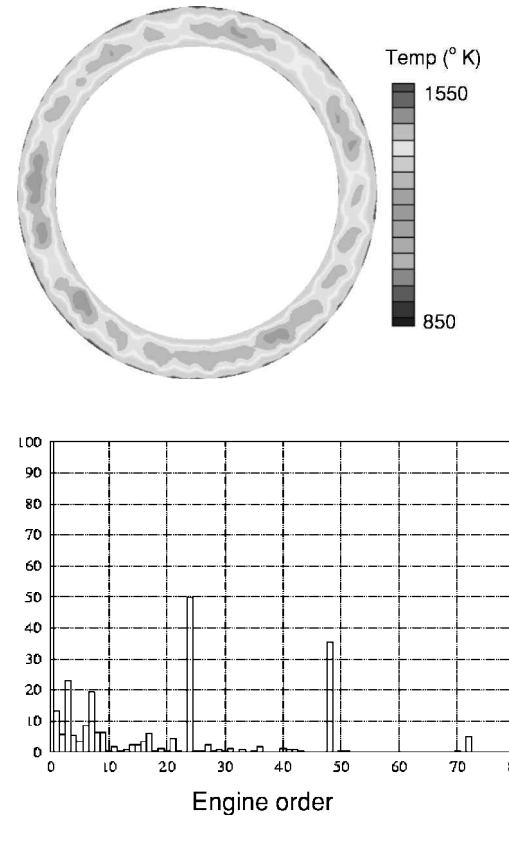

Fig. 3 TD at combustor exit and its Fourier transform at stator blade midspan.

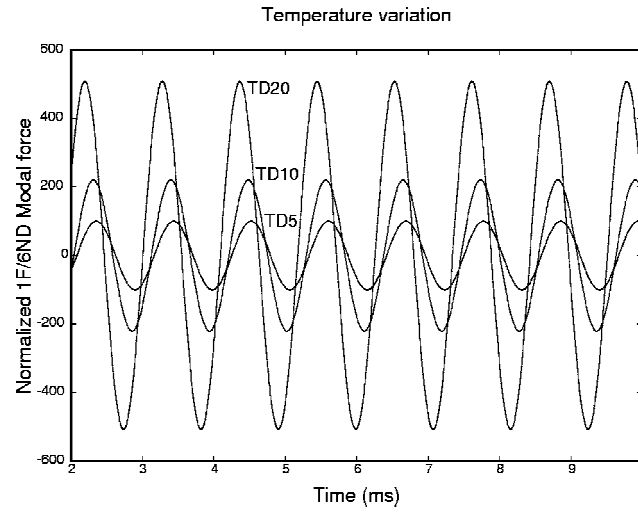

Fig. 4 Modal force time history for 5, 10, and 20% TD.

Effect of Temperature Distortion

Because of various combustion effects, the temperature at the exit of the combustor array is generally nonuniform, especially in the circumferential direction. Another common cause of severe temperature distortion is fully or partially blocked burners and this will be investigated later. Here we will use a representative temperature distribution under "normal" operating conditions, which is measured at the HP stator inlet (Fig. 3a). The corresponding Fourier transform at midspan is plotted in Fig. 3b. The high-order harmonics, namely, 24, 48, and 72 EOs, are due to the actual number of burners, which is 24. Of particular interest are the low harmonics, 4–7 EOs, whose amplitude can be as high as 25% of the highest (24 EO) harmonic.

Once a steady-state solution was obtained, time-accurate unsteady flow forced response computations were started by imposing the temperature distortion of Fig. 3 as a harmonic function of the pitch, with no amplitude variation in the radial direction. Initially, the peak-to-peak variation was chosen to be 10% of the mean temperature. The computation was terminated once a periodic solution was reached after several blade-passing periods. An inspection of the instantaneous entropy contours revealed that the temperature distortion was convected downstream, suggesting that several blade rows downstream may be affected by nonuniform combustion effects.

The computations were repeated for 5 and 20% temperature distortion, and the resulting periodically converged modal forces are plotted in Fig. 4. (Mesh convergence studies were conducted for the 20% distortion case by almost doubling the mesh size, and very little difference was observed between the two sets of results.) The amplitude of the modal force appears to be proportional to the amount of temperature distortion, though it may not be possible to generalize such behavior to other LEO parameters, especially for high-perturbation levels. In any case, a closer inspection of Fig. 4 reveals a more significant finding: There is a phase difference between the modal forces arising from the three temperature distortion cases, especially when the distortion amplitude is increased to 20 from 10%. As will be demonstrated later, such a feature has very important implications when studying the combined effects because excitation forces arising from individual parameters will either cancel each other out (in-phase case) or will produce much larger forcing by superposition (out-of-phase case).

Table 1 TW variation configurations: change from nominal width

Configuration	Passage 1,%	Passage 2,%	Passage 3,%	Passage 4,%	Passage 5,%	Passage 6,%
TW1	+3	+3	0	0	−3	−3
TW2	0	0	+3	+3	−3	−3
TW3	+3	+3	−3	−3	0	0

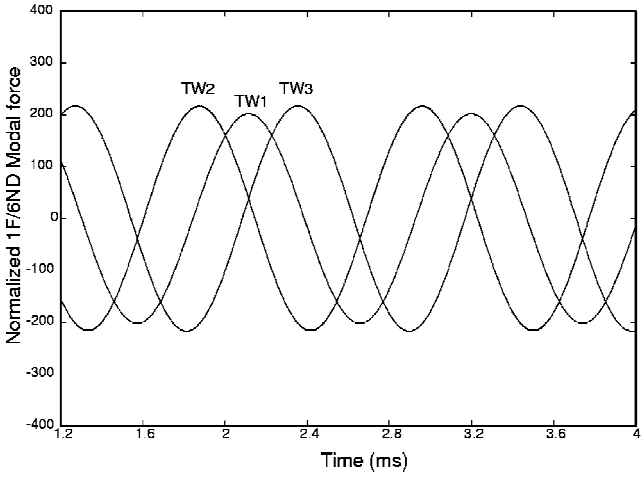

Fig. 5 Modal force time history for the three TW configurations.

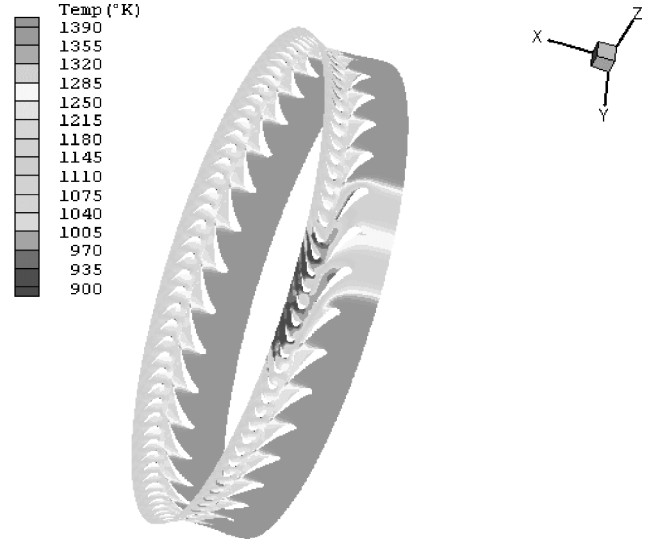

Fig. 6 Temperature contours at the tip section for configuration BB-1-2.

Effect of Stator Throat Width Variation

Another common cause of LEO excitation is aerodynamic mistuning arising from nonidentical stator blade passages due to manufacturing tolerances. Such variations, caused by manufacturing and assembly inaccuracies, can be characterised by increasing or decreasing the throat width (TW) between successive blades. A passage-to-passage difference of 3% is thought to be a representative value for the particular geometry under study. Three different configurations, TW1, TW2, and TW3, will be studied here (Table 1). For instance, referring to the typical sector with six stator blades, configuration TW1 consists of two blade passages with an increased TW of 3%, followed by two nominal passages, followed by two passages with a decreased TW of 3%. The meshing of such a configuration is not straightforward and requires the modification of the symmetric sector mesh by "moving" the stator blades with changed TWs. Note that TW2 and TW3 differ in phase only, whereas TW1 is effectively a mirror image. Such different configurations were considered to conduct combined parameter studies.

As before, the time-accurate forced response computations were initiated from a steady state solution of the sector model with the modified positions of the stator blades. The amplitude of the modal force, shown in Fig. 5, is about the same as for the 10% temperature distortion case. More significantly, as for the temperature distortion, there is a phase difference between the modal forces corresponding to the three stator configurations, confirming the significance of relative phasing between different excitations.

Effect of Flow Exit Angle

The flow exit angle may not be identical for all blades because of manufacturing and assembly tolerances. The typical sector of 6 stator and 15 rotor blades was also used for this study. As before, three different configurations, trailing edge TE1, TE2, and TE3, were studied by "rotating" individual blades by 0.3 deg about their midchord point. Such a value is considered to be within the expected range of flow exit angle variation. The magnitude of the modal force was found to be about the same as that for TW variations.

Effect of Blocked Burners

Although it is well established that fully or partially blocked burners create significant temperature distortions, the determination of the resulting LEO harmonics is not straightforward. Nevertheless, during rig tests, it is standard practice to block a number of burners and to try to assess the maximum LEO excitation.

The numerical simulation of an unsteady flow for an arbitrary number and position of blocked burners is not an easy task because whole-annulus models need to be used due to lack of symmetry. Furthermore, an accurate representation of the flowfield arising from a blocked burner requires the modeling of the combustors, a multidisciplinary problem that has not been fully solved yet for industrial configurations.[19] As shown in Fig. 6, the sector model of Fig. 2 was extended to a whole-annulus representation and measurement-based boundary conditions, the so-called cold streaks, were imposed at the HP nozzle guide vane (NGV) inlet. Strictly speaking, the blockage of a burner will affect not only the temperature but also the total pressure and flow angle. However, here we will consider the temperature distortion only and assume that the static and total pressure remain constant.

Here our aim is to determine the worst blocked burner configuration, giving rise to the highest low EO harmonic between 4 and 7. The total number of burners is 24. For the particular configuration under study, harmonics below 4 and above 7 are out of the engine running conditions for the resonance of the 1F/6ND vibration mode. Three different blocked burner (BB) patterns, BB-1-2, BB-1-2-13, and BB-1-13, were defined initially, the numbers referring to the positions of the blocked burners. A fourth configuration, BB-1-13C, was also studied by giving the two "cold spots" of configuration BB-1-13 a smaller circular-shape blockage. Such patterns were selected in the light of various industrial practices for engine endurance tests, although no established standards could be found. A spatial Fourier transform of each blockage pattern will reveal the harmonics that will be present in the excitation, although the magnitude can only be determined with an unsteady flow computation. For instance, pattern BB-1-2 will excite all harmonics, whereas pattern BB-1-13 will generate even-order harmonics only.

The LEO forced response calculations were conducted by including the first 10 nodal diameter assembly modes arising from the first blade mode (1F). The whole-annulus stator/rotor domain contained about 4.5 million points and the time step was chosen such that

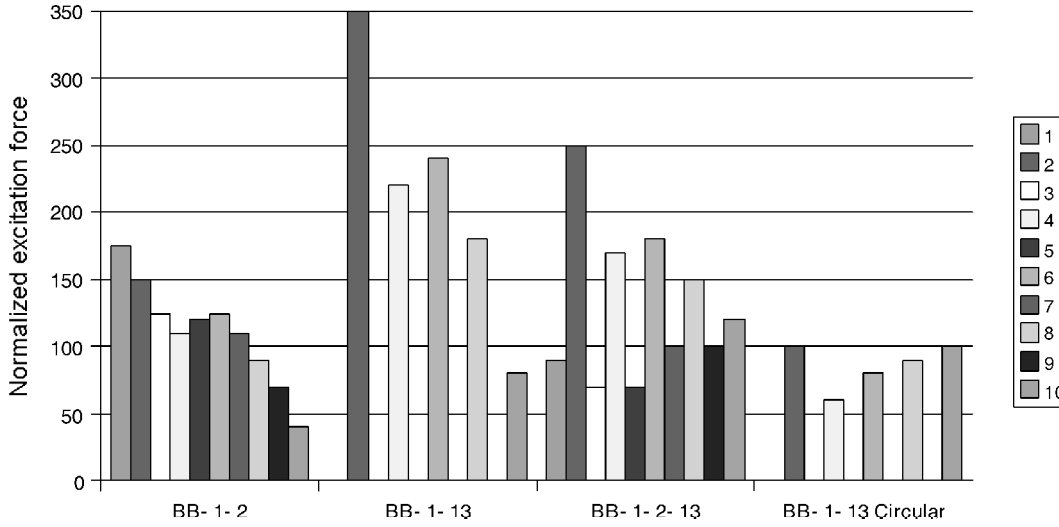

Fig. 7 Amplitude of modal forces for different BB configurations.

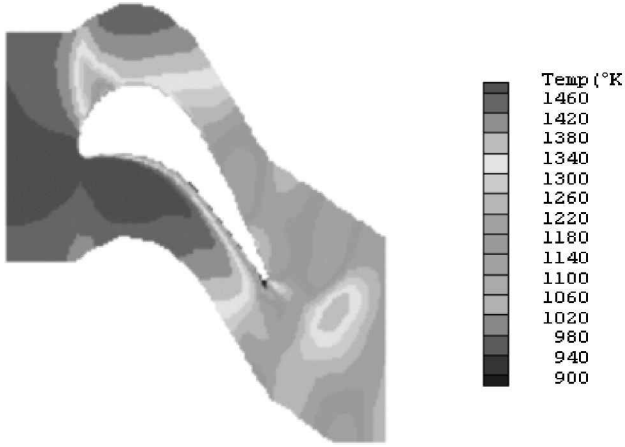

Fig. 8 Rotor blade temperature distribution with cooling flow.

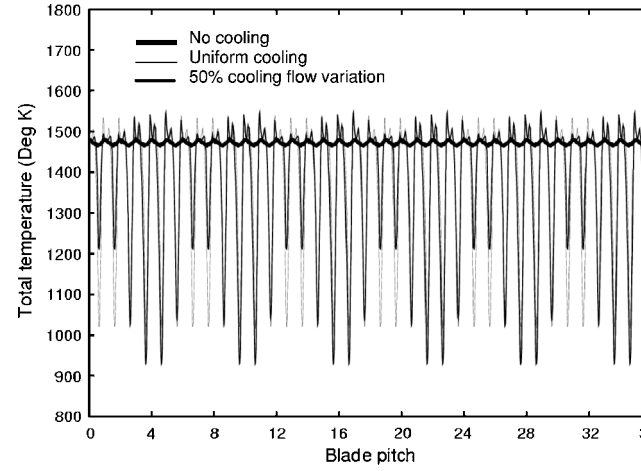

Fig. 9 Total temperature at NGV exit (75% height) with and without cooling.

the period of main blade-passing harmonic, 36 EO excitation, was defined with 40 points. The 6 EO harmonic, which is of main interest, will then be captured with 240 points, providing good temporal resolution. The total simulated time is over 1.5 full rotor revolutions. Each computation, run in parallel mode, took about 3 days (wall-clock time) on 16 R10000 CPUs of an SGi computer. The maximum modal force amplitude of the first 10 harmonics is shown in Fig. 7 for each of the four configurations. It is easily seen that pattern BB-1-13 produces the highest excitation levels. The actual shape and size of the cold spot are observed to be important parameters because the modal force amplitudes are markedly different for configurations BB-1-13 and BB-1-13C.

Effect of Cooling Flow Nonuniformities

The combustor exit temperature may be as high as 2000 K, and the HP turbine cannot operate without a cooling mechanism. Indeed, the cooling flow can be as much as 10% of the main flow. Although it is almost certain that there are significant cooling flow changes between the blades, the quantification of such nonuniformities is not straightforward. The cooling efficiency variation between the blades cannot be assessed easily, and the ensuing effects on blade forcing are totally unknown. Here the aim is to use a simple cooling flow model with a view to estimate the forcing effect, rather than to investigate the cooling efficiency on the blade surface.

The cooling flow injection was modeled via specific boundary conditions at the blade surface. The coolant temperature and normal velocity were specified as input. The cooling flow was assumed to impinge into the main flow at 90 deg. Therefore, only the normal momentum and the mass source terms were considered at the blade surface. In the particular case studied, the injection velocity was perturbed by up to 50% by imposing a 6 EO distortion. The total temperature distribution for the rotor domain is plotted in Fig. 8, an inspection of which reveals the presence of a film of cold air along the blade. With the imposed cooling flow perturbation, it was found that the mean value of the flow exit angle had shifted by about 0.7 deg. The total temperature distribution at 75% NGV height is plotted in Fig. 9 for three cases: no cooling, uniform cooling, and 6 EO distortion on cooling flow. As expected, there is no temperature variation across the pitch for the no-cooling flow case. On the other hand, when the cooling flow is uniform, the temperature variation is periodic with respect to each pitch. However, when the cooling flow is perturbed, the temperature variation deviates from this pattern, thus creating additional excitation harmonics. For the case under study, the 1F/6ND modal force reaches a normalized amplitude of about 800, the highest value for the parametric studies reported in this paper.

Study of Combined Effects

TW Variation and Temperature Distortion

In an aeroengine, most LEO excitation sources coexist together, and hence, it is very important to be able to assess if the combined effects can be inferred from the study of individual effects. Here we will focus on combined temperature distortion and TW variation effects because these are likely to be present in most situations.

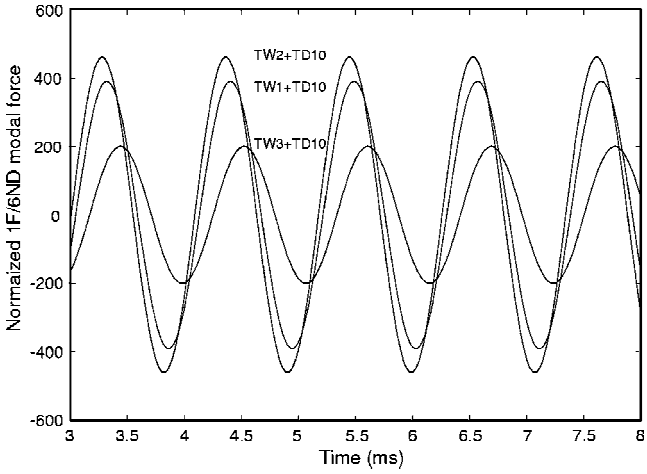

Fig. 10 Modal force time history for the three stator TW configurations plus TD10.

Because a detailed parametric study is likely to require massive computational resources, only a few combinations will be studied to establish general qualitative trends. The 10% temperature distortion (TD) case, TD10, was considered with each one of the earlier TW variation configurations, defined in Table 1. The resulting modal forces, plotted in Fig. 10, show a somewhat unexpected trend. It is seen that the amplitude of the modal force is much higher for configurations TW1 and TW2 than that for configuration TW3 in the presence of 10% TD. Because the modal force amplitude remains the same in all three TW variation cases when considered in isolation, the addition of the same TD might have been expected to produce similar modal force levels, which clearly is not the case here. However, as can be seen from Fig. 10, there is a significant phase difference between the three cases. Therefore, the amplitude of the total modal force will be governed by the phase differences between the modal forces due to individual excitations. This is a very important result because it can perhaps explain the marked LEO excitation differences between nominally identical engines. Both the TW variation and the TDs are likely to vary from engine to engine. Such a finding is very difficult to verify experimentally because of the lack of detailed information with existing documented case histories.

Further Combined Effects

A large number of combined parameter cases were studied using the typical stage sector of Fig. 2 with 6 stator and 15 rotor blades. The general trend will be illustrated by means of the following two examples: 1) temperature perturbation and flow exit angle variation (case TD10 plus case TE1) and 2) b) flow exit angle variation and TW variation (case TE2 plus case TW2).

The modal forces for the individual and combined cases are plotted in Figs. 11a and 11b. It is immediately seen that, as before, the phase between the modal forces of the individual cases is a key factor in governing the total excitation levels. For instance, Fig. 11a shows that the forcing due to combined TD10 plus TE3 effects is significantly lower than that for the individual components because these are out-of-phase with each other. On the other hand, Fig. 11b reveals a higher modal force for the combined case because the individual components are almost in-phase. In summary, the total excitation arising from the combined effects can be higher or lower than the forcing due to individual components, the key parameter being the phase difference between these components. In spite of considering several cases, it has not been possible to identify a pattern from which such phase changes can be inferred. As a result certain parameter combinations, such as one BB, plus TW variation, plus cooling flow variation, should probably studied together.

Wave-Splitting Analysis

The results of the preceding section indicate that the modal force due to the combined effects is determined by the phasing between

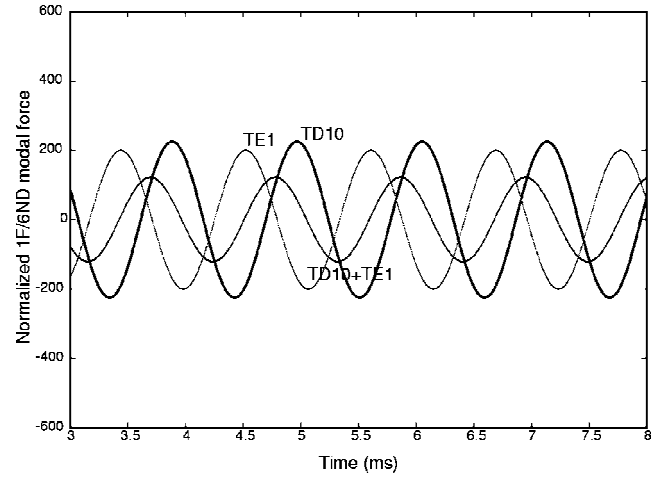

a) Combined TD 10 plus TE1 less than individual TD 10 and TE1

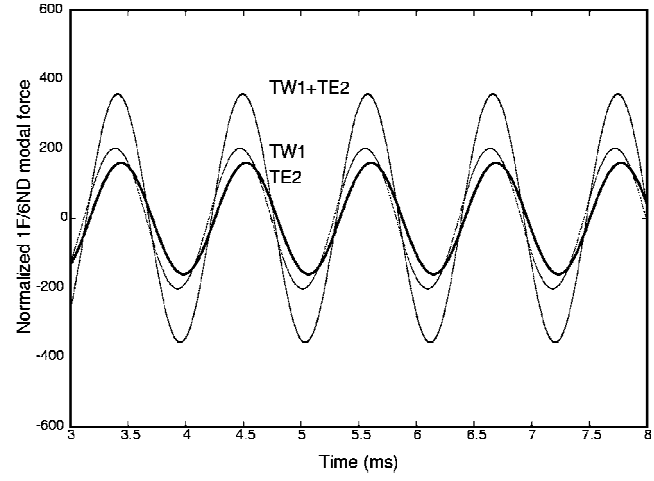

b) Combined TE2 plus TW2 greater than individual TE2 and TW2

Fig. 11 1F/6ND modal forcing for individual and combined parameters.

the individual excitations. Here we will study how each individual excitation contributes toward the elementary wave components, namely, entropy, vorticity, and potential. The elementary waves can be extracted from the steady-state flow at the NGV outlet using Goldstein's splitting theorem.[20] Figure 12 shows the wave decomposition for the TD10 case. There is a vorticity wave at the outflow, the phase difference between the vorticity and entropy waves being about 180 deg. The vorticity wave is due to velocity fluctuations created by TD, with hotter gas having a higher velocity. Because there is no change in the flow geometry, the amplitude of the pressure wave is nearly zero. As can be seen from Fig. 13, in the case of TW variation, there is no entropy wave. However, the vortical and pressure waves are of similar amplitude and have very similar phase. What is of interest here is the way the elementary waves are added under the combined effects. The wave split for the combined effects is shown in Fig. 14 for TD10 plus TW2. It is seen that the entropy wave from TD10 and the pressure wave from TW2 remain unchanged. Because only the vorticity wave appears to change as the result of LEO parameter interactions, the vorticity wave only is plotted in Fig. 15 for all three cases, namely, TW2, TD10, and TD10 plus TW2. Also plotted in Fig. 15 is the sum of the TD10 and TW2 vorticity waves, obtained by considering both the amplitude and the phase. It is seen that the vorticity wave from the combined case is almost identical to the sum of the individual vorticity waves, indicating that that the pressure and entropy waves are not important for this particular case. However, other cases, not reported here, showed that the sum of the individual vorticity waves could be significantly different from the vorticity wave of the combined case. Such a finding suggests that

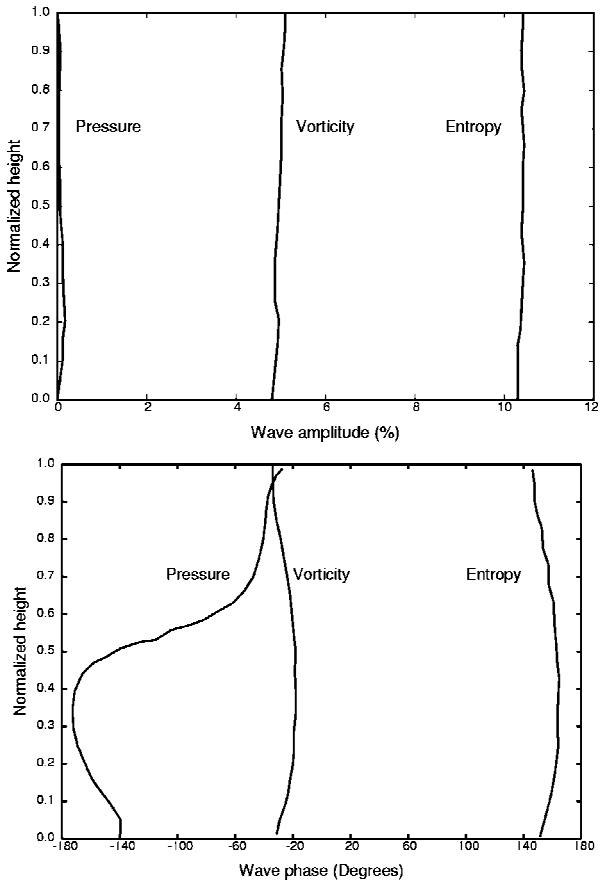

Fig. 12 Wave splitting for case TD10, amplitude and phase.

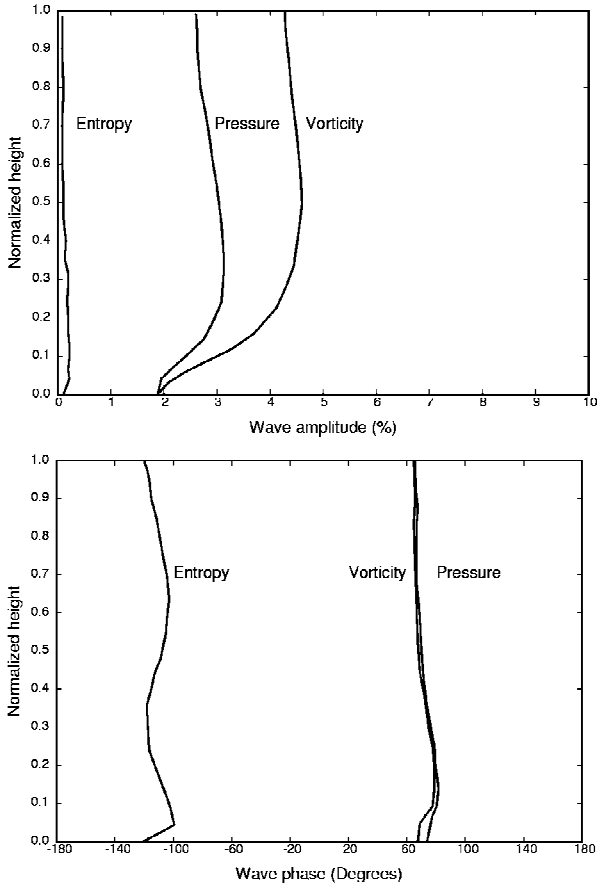

Fig. 13 Wave splitting for case TW2, amplitude and phase.

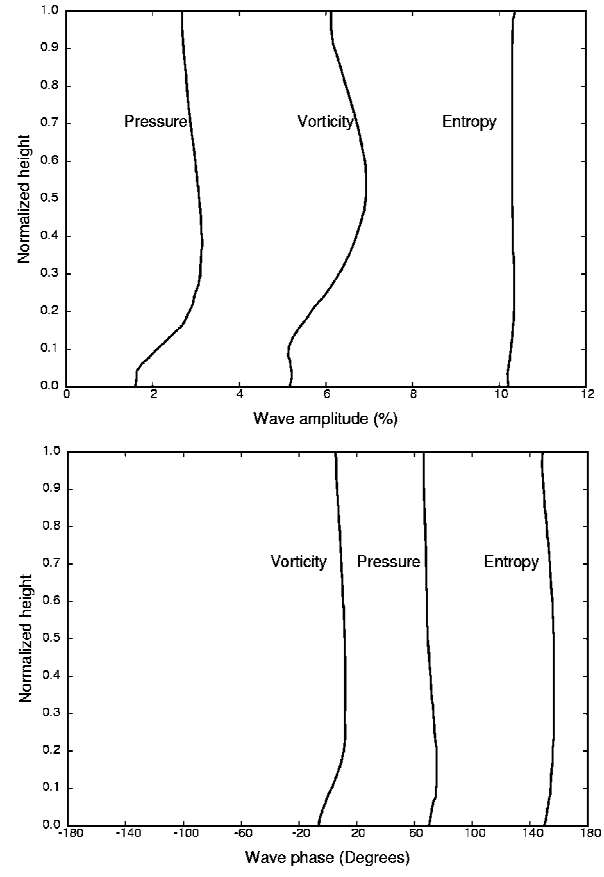

Fig. 14 Wave splitting for TD10 plus TW2, amplitude and phase.

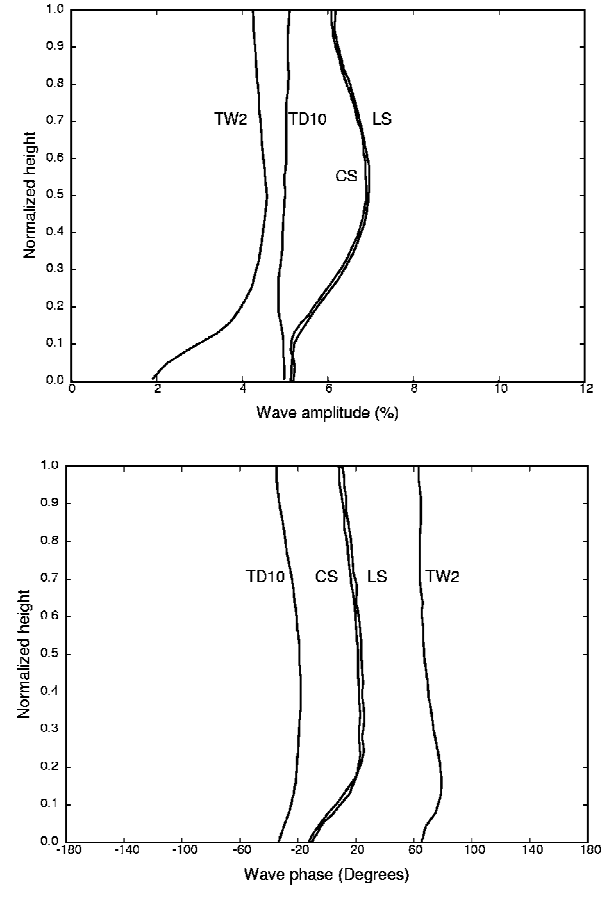

Fig. 15 Individual, linearly-superimposed (LS) and combined-case (CS) vorticity waves for TD10 plus TW2, amplitude and phase.

Table 2 Zero-to-peak modal force and actual displacement values for various computations

Case	Normalized force	Response normalized to equivalent blade-passing amplitude
5% TD, TD5	110	0.50
10% TD, TD10	220	1.00
20% TD, TD20	500	2.50
0.3 deg flow exit angle variation, configurations TE1, TE2, TE3	160–200	0.80–0.95
3% TW variation, configurations TW1, TW2, TW3	200–220	0.90–1.00
Cooling flow variation	800	3.70
B configuration 1 (1 and 2 blocked)	125	0.60
B configuration 2 (1, 2, and 13 blocked)	180	0.90
B configuration 3, (1 and 13 blocked)	240	1.20
Blocked burner configuration (Nos 1 & 13 blocked smaller footprint)	80	0.35
TW1 plus TD10	390	1.80
TW2 plus TD10	460	2.10
TW3 plus TD10	200	0.90
TD10 plus TE1	160	0.75
TD10 plus TW2	400	1.80
TE1 plus TW2	200	0.90
TE2 plus TW2	380	1.75

combined effects cannot always be deduced from knowledge of the individual cases. As a result, a nonlinear model, where all parameter perturbations are represented simultaneously, is likely to be needed to determine the vibration response to combined parameter cases.

Overview of Results and Comparison with Blade-Passing Excitation

The direct comparison of LEO response predictions with experimental data is a very difficult undertaking because of the need to quantity the variability of the controlling parameters such as throat width, flow exit angle, temperature distortion, etc. The values used in this numerical study are believed to be representative of variations that might be encountered in typical aeroengines. The matter is further complicated by the fact that is often impracticable to vary a single parameter only in actual engine assemblies. For instance, groups of NGV are often assembled around the annulus with gaps between them filled with a flexible material. Under operating conditions, uneven expansion of such gaps is likely to cause variations in the stator exit flow. For two different NGV configurations in terms of vane numbers and groupings, experimental evidence from development engines seems to link the number of vanes separated by gaps to the actual order of the excitation. However, the two configurations for which limited data are available have different numbers of burners, and so a direct comparison between them is not possible. Furthermore, the actual amount of passage-to-passage variations due to gap expansion cannot be quantified accurately under operating conditions. In any case, for EO 1–4, the LEO response was found to be about 50% of the corresponding blade-passing response, reducing to about 25% for orders 5–8. Here, the predicted response increase due to throat width and flow angle effects is about twice as high (about 100%), but some hardware details and the operating conditions are different. In another experimental study, measurements from development-engine test rigs showed a strong correlation with LEO response increase and burner blockage, the vibration levels being usually comparable to those from blade-passing excitation. Such an observation is consistent with the findings of the current numerical study. Finally, cooling flow variations are sometimes linked to very significant response increases, but there are no reliable experimental data, mainly because of the difficulties of quantifying cooling flow variations under operating conditions.

The numerical results of the preceding section are summarized in Table 2, where the normalized modal force for the 1F/6ND mode is listed for all cases studied. Also listed in Table 2 are the LEO displacement values, which are normalized with respect to the resonant amplitude arising from the main blade-passing excitation. A direct comparison is not possible because, at the same speed, the 36 EO blade-passing forcing will excite the first torsion 1T/36ND mode and not the 1F/6ND mode. Furthermore, a structural damping value of $Q = 50$ is assumed for both 1F/6EO and 1T/36EO modes. The values in the third column of Table 2 range between 0.5 and 3.70, indicating that the LEO response is not dissimilar to the equivalent blade-passing response, although it is stressed that the comparison requires considerable engineering judgement. In any case, given that there are large uncertainties with the quantification of the parameter perturbation levels and the assessment of damping under operating conditions, it may be concluded that blade-passing and LEO forced response amplitudes are comparable, a finding that is in line with observations during engine rig tests. However, it is possible that particular combinations of controlling parameters may yield significantly higher LEO forced response.

Conclusions

There are two types of LEO excitation. The first type can be classified as deterministic because it arises from given known conditions, such as inlet distortion for military engines or blade number differences in multistage assemblies. The second type, due to small configuration differences, is much less foreseeable because of the unknown variability of the controlling parameters. This paper has been focused on the latter, and the following observations can be made.

1) Broadly speaking, for a given parameter, the LEO forcing increase appears to be proportional to the amount of perturbation in that parameter, although more studies are needed to confirm this finding, especially for high levels of perturbation. Regarding the worst BB configuration, the blocking of two consecutive burners appears to produce the largest response levels, although the results depend on the actual definition of the cold spots.

2) It is difficult to determine the most critical LEO excitation because the quantification of the parameter variation levels is not straightforward. When is assumed that the distributions used in this study are representative of engine conditions, it can be concluded that 10% TD, 3% TW variation, 0.3-deg flow angle variation, or the blocking of two consecutive burners are likely to produce the same vibration levels. Although the cooling flow effects are seen to be the largest, the imposed 50% velocity variation is probably an upper limit. Again, a variation of 10% is likely to give similar response levels.

3) It has been found that knowledge of individual excitation cases is not sufficient for determining the response levels due to combined effects by simple linear superposition. Such nonlinear behavior is also exhibited when adding the elementary pressure, vorticity, and entropy waves arising from individual excitation cases, although more work is needed to explain the exact physical mechanisms. In

any case, the relative phase between individual excitation sources is a key factor for the overall excitation levels. Such a finding is consistent with the markedly different LEO response behavior of nominally identical engines because the variations of the controlling parameters are likely to be different from engine to engine.

4) A ballpark comparison of the blade-passing and LEO forced response suggests similar vibration levels in both cases. Such a finding is consistent with current engine experience, which indicates that about half of the high-cycle fatigue problems are caused by LEO response.

Acknowledgments

The authors would like to thank the U.K. Engineering and Physical Sciences Research Council (GR/M21652) for funding the work and Rolls–Royce, plc., for providing some of the data. Thanks are also due to Robert Elliott of Rolls–Royce, plc., for many useful discussions.

References

[1]Griffin, J. H., and Hosac, T. M., "Model Development and Statistical Investigation of Turbine Blade Mistuning," *Journal of Vibration, Acoustics and Stress and Reliability in Design*, Vol. 106, No. 2, 1984, pp. 204–210.

[2]Petrov, E. P., Sanliturk, K. Y., and Ewins, D. J., "A New Method for Dynamic Analysis of Mistuned Bladed Disks Based on the Exact Relationship Between Tuned and Mistuned Systems," *Journal of Engineering for Gas Turbines and Power*, Vol. 124, No. 5, 2002, pp. 586–597.

[3]Chiang, H. D., and Kielb, R. E., "An Analysis System for Blade Forced Response," American Society of Mechanical Engineers, ASME Paper 92-GT-172, June 1992.

[4]Hodson, H. P., "An Inviscid Blade-to-Blade Prediction of a Wake-Generated Unsteady Flow," American Society of Mechanical Engineers, ASME Paper 84-GT-43, May 1984.

[5]Giles, M. B., "Calculation of Unsteady Wake/Rotor Interaction," *Journal of Propulsion*, Vol. 4, No. 3, 1988, pp. 356–362.

[6]Fransson, T. H., and Pandolfi, M., "Numerical Investigation of Unsteady Subsonic Compressible Flows Through an Oscillating Cascade," American Society of Mechanical Engineers, ASME Paper 86-GT-304, June 1986.

[7]Gerolymos, G. A., "Numerical Integration of the Blade-to-Blade Surface Euler Equations in Vibrating Cascades," *AIAA Journal*, Vol. 26, No. 9, 1988, pp. 1483–1492.

[8]Rai, M., "Unsteady 3D Navier–Stokes Simulations of Turbine Rotor–Stator Interaction," AIAA Paper 87-2038, June 1987.

[9]Korakianitis, T., "On the Prediction of Unsteady Forces on Gas Turbine Blades—Part 1," American Society of Mechanical Engineers, ASME Paper 88-GT-89, June 1988.

[10]Korakianitis, T., "On the Prediction of Unsteady Forces on Gas Turbine Blades—Part 2," American Society of Mechanical Engineers, ASME Paper 8-GT-1988, June 1988.

[11]Manwearing, S. R., and Wisler, D. C., "Unsteady Aerodynamics and Gust Response in Compressors and Turbines," American Society of Mechanical Engineers, ASME Paper 92-GT-422, June 1992.

[12]Manwearing, S. R., and Kirkeng, K. L., "Forced Response Vibrations of a LP Turbine due to Circumferential Temperature Distortions," *Unsteady Aerodynamics and Aeroelasticity of Turbomachines*, edited by T. H. Fransson, Kluwer Academic, Dordrecht, The Netherlands, 1998, pp. 641–654.

[13]Sayma, A. I., Vahdati, M., and Imregun, M., "Multi-stage Whole-Annulus Forced Response Predictions Using an Integrated Non-linear Analysis Technique—Part I: Numerical Model," *Journal of Fluids and Structures*, Vol. 14, No. 1, 2000, pp. 87–101.

[14]Vahdati, M., Sayma, A. I., and Imregun, M., "Multi-stage Whole-Annulus Forced Response Predictions Using an Integrated Non-linear Analysis Technique—Part II: Study of a HP Turbine," *Journal of Fluids and Structures*, Vol. 14, No. 1, 2000, pp. 103–125.

[15]Sayma, A. I, Vahdati, M., Sbardella, L., and Imregun, M., "Modeling of Three-Dimensional Viscous Compressible Turbomachinery Flows Using Unstructured Hybrid Grids," *AIAA Journal*, Vol. 38, No. 6, 2000, pp. 945–954.

[16]Sayma, A., Vahdati, M., and Imregun, M., "Turbine Forced Response Prediction Using an Integrated Non-linear Analysis," *Journal of Multi-body Dynamics*, Vol. 214, No. K1, 2000, pp. 45–60.

[17]Barakos, G., Vahdati, M., Sayma, A. I., Bréard, C., and Imregun, M., "A Fully-Distributed Unstructured Navier–Stokes Solver for Large-Scale Aeroelasticity Computations," *Aeronautical Journal*, Vol. 105, No. 1050, 2001, pp. 419–426.

[18]Sbardella, L., Sayma, A. I., and Imregun, M., "Semi–Structured Meshes for Axial Turbomachinery Blades," *International Journal for Numerical Methods in Fluids*, Vol. 32, No. 5, 2000, pp. 569–584.

[19]Bréard, C., Sayma, A., Vahdati, M., and Imregun, M., "Aeroelasticity Analysis of an Industrial Gas Turbine Combustor," *Journal of Fluids and Structures*, Vol. 16, No. 8, 2002, pp. 1111–1126.

[20]Goldstein, M. E., "Unsteady Vortical and Entropic Distortions of Potential Flows Round Arbitrary Obstacles," *Journal of Fluid Mechanics*, Vol. 89, No. 2, 1978, pp. 433–468.